Synthesis and Characterization of Coil−Rod−Coil Triblock Copolymers Comprising Fluorene-Based Mesogenic Monodisperse Conjugated Rod and Poly(ethylene oxide) Coil

Laju Bu,[†,‡] Yao Qu,[†] Donghang Yan,[†] Yanhou Geng,*[,†] and Fosong Wang[†]

State Key Laboratory of Polymer Physics and Chemistry, Changchun Institute of Applied Chemistry, Chinese Academy of Sciences, Changchun 130022, P. R. China, and Graduate School of Chinese Academy of Sciences, Beijing 100049, P. R. China

Received November 19, 2008; Revised Manuscript Received December 16, 2008

ABSTRACT: A series of coil−rod−coil triblock copolymers (i.e., **F3T8EO8**, **F3T8EO17**, **F3T8EO45**, and **F3T8EO125**) with a mesogenic monodisperse conjugated oligomer comprising 3 fluorene, 8 thiophene, and 2 phenyl units as the rod and poly(ethylene oxide) (PEO) as the coil were synthesized. A reference compound, that is **F3T8ME2**, with the identical rod but without PEO was also prepared for comparison. The volume fraction of PEO (f_{PEO}) was 0, 0.16, 0.28, 0.50, and 0.73 for **F3T8ME2, F3T8EO8**, **F3T8EO17**, **F3T8EO45**, and **F3T8EO125**, respectively. It was found that the introduction of PEO into the triblock copolymers encouraged the formation of H-type aggregation and f_{PEO}-dependent highly ordered mesophases while $f_{PEO} < 0.73$. For **F3T8ME2**, only nematic mesophase was observed. In contrast, **F3T8EO8** and **F3T8EO17**, with f_{PEO} of 0.16 and 0.28, respectively, are smectic A (S_A) mesomorphism. For **F3T8EO45** with f_{PEO} of 0.50, several highly ordered phases, such as hexagonal columnar crystalline phase and rectangular columnar, smectic B (S_B) and S_A mesophases, appear in succession upon heating. However, large f_{PEO} suppresses the formation of mesophase. For **F3T8EO125** with $f_{PEO} = 0.73$, only a crystalline phase was observed. Meanwhile, thin films of above triblock copolymers exhibit lamellar or cylindrical nanostructures consistent with the phase structures at room temperatures, which render the block copolymers different spectroscopic properties. These results indicate that it is possible to control the supramolecular nanostructures of conjugated materials and then to tune their optoelectronic properties by designing rod−coil block copolymers with appropriate chemical structures.

Introduction

Supramolecular nanostructures of conjugated materials play a crucial role in their optoelectronic properties,[1] and integration of the conjugated rod segments and flexible coils to form rod−coil block copolymers has been proved as an effective way to control the supramolecular nanostructures of conjugated materials and then to tune the optoelectronic properties.[2−5] It was found that rod−coil molecules could self-organize into one- to three-dimensional supramolecular nanostructures by variation of the coil to rod volume ratio.[3,6,7] For example, liquid crystalline rod−coil block copolymers can form unconventional mesophases including hexagonal columnar, rectangular columnar, bicontinuous cubic, perforated layer, and body-centered tetragonal phases, in addition to nematic, smectic, and cholesteric ones.[7,8] Particularly, rodlike conjugated segments prefer to form mesophases or other special aggregates driven by miscellaneous molecular interactions such as $\pi-\pi$ interaction, which can in principle endow the rod−coil block copolymers strong phase separation and assembling properties. Several series of liquid crystalline rod−coil block polymers based-on well-defined conjugated rod segments, such as oligo(phenylenevinylene)s (OPVs),[9−11] oligophenylenes (OPhs),[12] and phenylene/fluorene/thiophene hybride oligomers,[13] have been reported to be capable of forming molecular-structure-related supramolecular nanostructures. For example, Yu et al. synthesized liquid crystalline diblock and triblock copolymers comprising OPV rod and poly(ethylene oxide) (PEO) coil, which exhibited unidentified lowly ordered mesophase.[9] In contrast, the conjugated rod-based block copolymers reported by Stupp[11] and Lin,[13] in which rod segments were asymmetrically end-substituted with a hydrophobic alkyl chain and hydrophilic PEO, can self-organize into a variety of highly ordered mesophases.

Fluorene-based polymers are of great interest in recent years because of their applications in optoelectronic devices (such as organic light-emitting diodes, organic thin-film transistors, and organic solar cells) and ease of molecular-structure modulation.[14−21] Typically, they are well-known as the hairy-rod nematic liquid crystals. Several rod−coil or coil−rod−coil block copolymers have been developed with fluorene-based polymers[22−29] or short oligomers as rod segment.[30−34] In these reports, polydispersity indices (PDIs) of polyfluorenes are >1.5 due to limitation of the polymerization method, and short oligofluorenes are nonmesogenic due to their short conjugation length. Therefore, they are intrinsically not appropriate building blocks for block copolymers capable of forming well-defined supramolecular nanostructures, although some of the block polymers have been found to exhibit fiberlike or lamellar film morphologies.[25,26,29] In fact, no fluorene-based block copolymers for tuning thermotropic liquid crystalline properties are reported yet. On the other hand, monodisperse conjugated oligomers (MCOs) have been intensively studied for establishing structure−property relationship in recent years.[35] In principle, their uniform and well-defined molecular structures also qualify them as ideal building blocks for block copolymers capable of forming well-defined supramolecular nanostructures. Particularly, fluorene-based MCOs are also mesomorphism while the molecular length is beyond a critical value,[36−39] and introduction of long alkyl chains at the terminals of short oligofluorenes can also render them mesomorphism.[40] In previous report, we have shown that oligo(fluorene-*alt*-bithiophene)s (OFbTs) longer than **F4Th6** (four fluorenes and three bithiophenes)

* Corresponding author. E-mail: yhgeng@ciac.jl.cn.
† Chinese Academy of Sciences.
‡ Graduate School of Chinese Academy of Sciences.

10.1021/ma802601c CCC: $40.75
Published on Web 02/09/2009

are nematic liquid crystals,[39] and meanwhile, poly(fluorene-*alt*-bithiophene) is one of the most promising semiconducting polymers due to its excellent stability against oxidation and high charge carrier mobility.[41,42] Therefore, herein we design and synthesize a series of coil−rod−coil triblock copolymers with an OFbT-type MCO as the rod segment and poly(ethylene oxide)s (PEOs) with different molecular weight as the coil segments. Effect of PEO volume fractions (f_{PEO}, calculated according to the reference by assuming the densities of OFbT[43] and PEO[44] segments are 1.14 and 1.13 g/cm^3, respectively) on photophysical, thermotropic, and phase separation properties of the resulting PEO-*b*-OFbT-*b*-PEO triblock copolymers are systematically investigated.

Experimental Section

Materials. PEOs with weight-average molecular weights (M_w) = 350, 750, 2000, and 5000 and PDIs of 1.15, 1.21, 1.23, and 1.27, respectively, were purchased from Aldrich Chemical Co. Compounds **1** and **4** were synthesized according to our previous report.[39] 4-(Dimethylamino)pyridinium 4-toluenesulfonate (DPTS) was prepared according to the literature.[45,46] Tetrahydrofuran (THF) and toluene were distilled from sodium/benzophenone. *N*,*N*-Dimethylformamide (DMF) was distilled from CaH_2 under reduced pressure. Methylene chloride was distilled over CaH_2. Other reagents were obtained from commercial sources and used without further purification.

Compound **3**. In the absence of light, a solution of compound **1** (7.00 g, 7.59 mmol), methyl 4-iodobenzoate (**2**) (3.98 g, 15.17 mmol), and $Pd(PPh_3)_4$ (87.7 mg, 7.59×10^{-2} mmol) in anhydrous DMF/toluene (40 mL, v/v = 1:4) was stirred for 24 h at 70 °C. The mixture was cooled to room temperature and then poured into a large amount of water for extraction with methylene chloride. The organic extracts were washed with aqueous KF solution and brine before being dried over $MgSO_4$. Upon evaporating off the solvent, the residue was purified with column chromatography on silica gel with petroleum ether/methylene chloride (1/3) as eluent to afford **3** as a yellow solid (4.08 g, 70%). ^{1}H NMR (300 MHz, $CDCl_3$): δ 8.09 (d, J = 8.49 Hz, 2H), 7.73 (m, 3H), 7.64−7.56 (m, 3H), 7.51−7.48 (m, 2H), 7.41 (d, J = 3.81 Hz, 1H), 7.35 (d, J = 3.78 Hz, 1H), 7.26 (dd, J = 2.49 Hz, J = 3.76 Hz, 2H), 3.97 (s, 3H), 2.04−1.97 (m, 4H), 1.25−1.10 (m, 20H), 0.85 (t, J = 6.70 Hz, 6H), 0.67 (m, 4H).

F3T8ME2. In the absence of light, a solution of compounds **3** (2.04 g, 2.66 mmol) and **4** (1.38 g, 1.06 mmol) and $Pd(PPh_3)_4$ (24.6 mg, 2.12×10^{-2} mmol) in anhydrous DMF/toluene (40 mL, v/v = 1/4) was stirred for 24 h at 85 °C. The mixture was cooled to room temperature and then poured into a large amount of water for extraction with methylene chloride. The organic extracts were washed with aqueous KF solution and brine before being dried over $MgSO_4$. Upon evaporating off the solvent, the residue was purified with column chromatography on silica gel with petroleum ether/methylene chloride (1/1) as eluent and further with PGPC to afford **F3T8ME2** as a yellow solid (1.50 g, 66%). ^{1}H NMR (400 MHz, $CDCl_3$): δ 8.05 (d, J = 8.43 Hz, 4H), 7.68 (m, 10H), 7.62 (m, 6H), 7.57 (m, 6H), 7.36 (d, J = 3.8 Hz, 2H), 7.33 (m, 6H), 7.22 (m, 8H), 3.94 (s, 6H), 2.04 (m, 12H), 1.20−1.09 (m, 60H), 0.80 (t, J = 6.66 Hz, 18H), 0.64 (m, 12H). MS (MALDI-TOF, reflection mode): m/z (%): 2091.78 (100) $[M]^+$. Elemental analysis (%) calcd for $C_{135}H_{150}O_4S_8$ (2091.93): C 77.46, H 7.22; found: C 77.26, H 7.49.

Compound **5**. 11 mL of 1 mol/L KOH aqueous solution was dropped into 100 mL of compound **3** (4.00 g, 5.21 mmol) THF solution. The mixture was then stirred at 80 °C for 10 h. After being cooled to room temperature, the reaction mixture was dropped into 300 mL of 2 mol/L HCl. Yellow flakes floated on the solution surface and were collected by filtration and then dried in vacuum at 70 °C to afford **5** (3.93 g, 100%). ^{1}H NMR (300 MHz, $CDCl_3$): δ 8.11 (d, J = 8.46 Hz, 2H), 7.73 (d, J = 8.46 Hz, 2H), 7.66 (d, J = 7.98 Hz, 1H), 7.58 (dd, J = 1.50 Hz, J = 7.96 Hz, 1H), 7.75 (d, J = 8.70 Hz, 2H), 7.47−7.43 (m, 2H), 7.38 (d, J = 3.81 Hz, 1H), 7.31 (d, J = 3.87 Hz, 1H), 7.23 (dd, J = 2.22 Hz, J = 3.72 Hz, 2H), 2.04−1.93 (m, 4H), 1.25−1.08 (m, 20H), 0.85 (t, J = 6.90 Hz, 6H), 0.64 (m, 4H).

Compound **6**. Compounds **6a**−**d** were synthesized in the same manner, so a representative procedure is described for **6a**. 0.23 g (0.66 mmol) of PEO (M_w = 350) was first dried by azeotropic distillation with anhydrous toluene, and then toluene was evacuated. Acid **5** (0.47 g, 0.62 mmol) in 20 mL of anhydrous methylene chloride was added, and then DPTS (0.19 g, 0.66 mmol) and dicyclohexyl carbodiimde (DCC) (0.19 g, 0.94 mmol) in 5 mL of anhydrous methylene chloride was added dropwise. The mixture was stirred at room temperature for 24 h and then filtered. The filtrate was washed with water and dried with $MgSO_4$. After evaporation of the solvent, the residue was purified with column chromatography on silica gel with methylene chloride/methanol (20:1) as eluent to afford **6a** as a sticky yellow solid (0.58 g, 86%). ^{1}H NMR (300 MHz, $CDCl_3$): δ 7.98 (d, J = 8.31 Hz, 2H), 7.58 (d, J = 8.28 Hz, 3H), 7.58 (dd, J = 1.47 Hz, J = 7.86 Hz, 1H), 7.55 (d, J = 8.58 Hz, 1H), 7.51 (m, 2H), 7.46−7.43 (m, 2H), 7.36 (d, J = 3.81 Hz, 1H), 7.30 (d, J = 3.78 Hz, 1H), 7.22 (dd, J = 2.52 Hz, J = 3.69 Hz, 2H), 4.48 (t, J = 4.80 Hz, 2H), 3.84 (t, J = 4.80 Hz, 2H), 3.70−3.60 (m, 22.8H), 3.55−3.51 (m, 2H), 3.36 (s, 3H), 1.99−1.93 (m, 4H), 1.24−1.05 (m, 20H), 0.80 (t, J = 6.80 Hz, 6H), 0.64 (m, 4H).

Compound **6b**. Yield: 75%. ^{1}H NMR (300 MHz, $CDCl_3$): δ 8.05 (d, J = 8.37 Hz, 2H), 7.65 (d, J = 8.25 Hz, 3H), 7.58 (dd, J = 1.41 Hz, J = 7.89 Hz, 1H), 7.54 (d, J = 8.04 Hz, 1H), 7.52 (m, 2H), 7.46−7.44 (m, 2H), 7.36 (d, J = 3.87 Hz, 1H), 7.31 (d, J = 3.84 Hz, 1H), 7.22 (dd, J = 2.52 Hz, J = 3.69 Hz, 2H), 4.48 (t, J = 4.80 Hz, 2H), 3.84 (t, J = 4.80 Hz, 2H), 3.70−3.60 (m, 60.4H), 3.55−3.52 (m, 2H), 3.37 (s, 3H), 1.99−1.93 (m, 4H), 1.24−1.05 (m, 20H), 0.80 (t, J = 6.80 Hz, 6H), 0.63 (m, 4H).

Compound **6c**. Yield: 82%. ^{1}H NMR (300 MHz, $CDCl_3$): δ 8.05 (d, J = 8.37 Hz, 2H), 7.65 (d, J = 8.25 Hz, 3H), 7.58 (dd, J = 1.41 Hz, J = 7.89 Hz, 1H), 7.54 (d, J = 8.04 Hz, 1H), 7.52 (m, 2H), 7.46−7.44 (m, 2H), 7.36 (d, J = 3.87 Hz, 1H), 7.31 (d, J = 3.84 Hz, 1H), 7.22 (dd, J = 2.52 Hz, J = 3.69 Hz, 2H), 4.48 (t, J = 4.80 Hz, 2H), 3.84 (t, J = 4.80 Hz, 2.5H), 3.69−3.37 (m, 187.2H), 3.36 (s, 3H), 1.97−1.93 (m, 4H), 1.22−1.05 (m, 20H), 0.80 (t, J = 6.80 Hz, 6H), 0.63 (m, 4H).

Compound **6d**. Yield: 75%. ^{1}H NMR (300 MHz, $CDCl_3$): δ 8.05 (d, J = 8.37 Hz, 2H), 7.65 (d, J = 8.25 Hz, 3H), 7.58 (dd, J = 1.41 Hz, J = 7.89 Hz, 1H), 7.54 (d, J = 8.04 Hz, 1H), 7.52 (m, 2H), 7.46−7.44 (m, 2H), 7.36 (d, J = 3.87 Hz, 1H), 7.31 (d, J = 3.84 Hz, 1H), 7.22 (dd, J = 2.52 Hz, J = 3.69 Hz, 2H), 4.48 (t, J = 4.80 Hz, 2H), 3.85 (m, 4.6H), 3.71−3.38 (m, 419.5H), 3.37 (s, 3H), 1.95 (m, 4H), 1.22−1.05 (m, 20H), 0.80 (t, J = 6.80 Hz, 6H), 0.63 (m, 4H).

PEO-b-OFbT-b-PEO Triblock Copolymers. Triblock copolymers were synthesized in the same manner, so a representative procedure is described for **F3T8EO8**. In the absence of light, a solution of compound **4** (0.32 g, 0.25 mmol), **6a** (0.58 g, 0.54 mmol), and $Pd(PPh_3)_4$ (5.7 mg, 4.90×10^{-3} mol) in anhydrous DMF/toluene (5 mL, v/v = 1:4) was stirred for 24 h at 85 °C. The mixture was dried in vacuum at 100 °C and then purified with column chromatography on silica gel with methanol/methylene chloride (1:20) as eluent. The residue was further purified with PGPC to afford **F3T8EO8** as a yellow sticky solid (0.20 g, 30%). ^{1}H NMR (400 MHz, $CDCl_3$): δ 8.07 (d, J = 8.40 Hz, 4H), 7.70 (d, J = 8.00 Hz, 6H), 7.67 (d, J = 8.40 Hz, 4H), 7.62 (m, 6H), 7.57 (m, 6H), 7.37 (d, J = 4.00 Hz, 2H), 7.34 (m, 6H), 7.24 (m, 8H), 4.50 (t, J = 4.60 Hz, 4H), 3.86 (t, J = 4.80 Hz, 4H), 3.73−3.63 (m, 53.1H), 3.54 (t, J = 4.60 Hz, 4H), 3.38 (s, 6H), 2.05 (m, 12H), 1.20−1.09 (m, 60H), 0.80 (t, J = 6.80 Hz, 18H), 0.64 (m, 12H). Elemental analysis (%) calcd for $C_{168.1}H_{216.2}O_{20.6}S_8$ (2822.7) based on ^{1}H NMR spectrum: C 71.54, H 7.72; found: C 71.56, H 7.72.

F3T8EO17. Yield: 40% (0.30 g, yellow sticky solid). ^{1}H NMR (400 MHz, $CDCl_3$): δ 8.07 (d, J = 8.40 Hz, 4H), 7.70 (d, J = 7.6 Hz, 6H), 7.67 (d, J = 8.4 Hz, 4H), 7.62 (m, 6H), 7.57 (m, 6H), 7.38 (d, J = 4.0 Hz, 2H), 7.34 (m, 6H), 7.24 (m, 8H), 4.50 (t, J = 4.60 Hz, 4H), 3.86 (t, J = 4.60 Hz, 4H), 3.73−3.63 (m, 120.2H),

Scheme 1. Synthetic Route of Reference Compound F3T8ME2 and PEO-*b*-OFbT-*b*-PEO Triblock Copolymers F3T8EO8, F3T8EO17, F3T8EO45, and F3T8EO125[a]

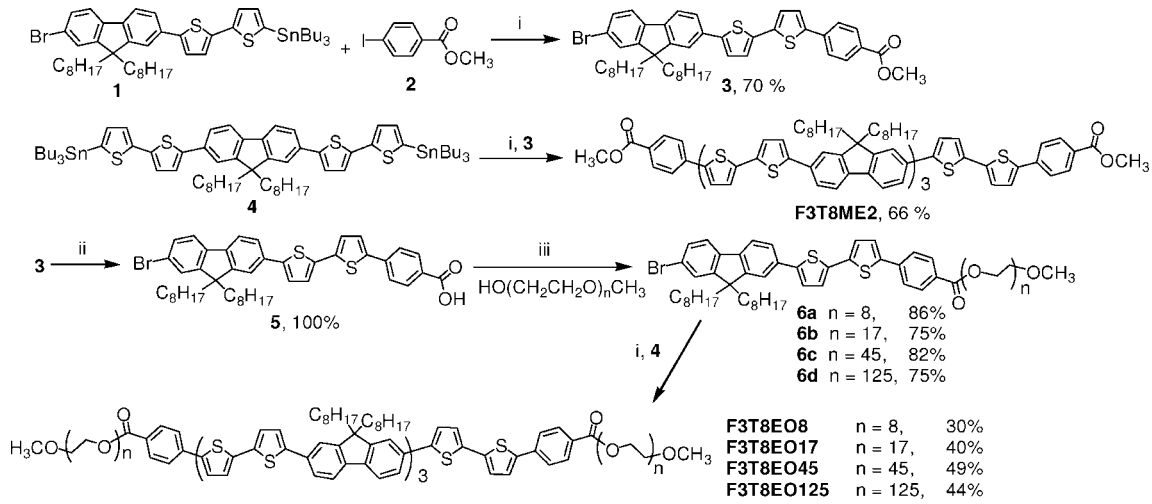

[a] (i) $Pd(PPh_3)_4$, toluene/DMF (volume 4/1), 70 or 85 °C. (ii) (1) KOH, H_2O, reflux; (2) HCl (2.0 M). (iii) DPTS/DCC, CH_2Cl_2, room temperature. DMF = *N*,*N*-dimethylformamide; DPTS = 4-(dimethylamino)pyridinium 4-toluenesulfonate; DCC = dicyclohexylcarbodiimide.

3.54 (t, J = 4.0 Hz, 4H), 3.38 (s, 6H), 2.04 (m, 12H), 1.20−1.09 (m, 60H), 0.80 (t, J = 6.8 Hz, 18H), 0.64 (m, 12H). Elemental analysis (%) calcd for $C_{203.6}H_{287.3}O_{38.3}S_8$ (3605.0) based on ^{1}H NMR spectrum: C 67.85, H 8.03; found: C 67.82, H 8.26.

F3T8EO45. Yield: 49% (0.46 g, yellow solid). ^{1}H NMR (400 MHz, $CDCl_3$): δ 8.07 (d, J = 8.40 Hz, 4H), 7.70 (d, J = 7.6 Hz, 6H), 7.67 (d, J = 8.4 Hz, 4H), 7.62 (m, 6H), 7.57 (m, 6H), 7.38 (d, J = 4.0 Hz, 2H), 7.34 (m, 6H), 7.24 (m, 8H), 4.50 (t, J = 4.60 Hz, 4H), 3.87−3.74 (m, 6H), 3.73−3.59 (m, 345.0H), 3.55 (m, 4H), 4.45 (t, J = 4.80 Hz, 2H), 3.38 (s, 6H), 2.04 (m, 12H), 1.20−1.09 (m, 60H), 0.80 (t, J = 6.8 Hz, 18H), 0.64 (m, 12H). Elemental analysis (%) calcd for $C_{315.5}H_{511.0}O_{94.2}S_8$ (6068.5): C 62.44, H 8.49; found: C 62.87, H 8.45.

F3T8EO125. Yield: 44% (0.46 g, yellow solid). ^{1}H NMR (400 MHz, $CDCl_3$): δ 8.07 (d, J = 8.40 Hz, 4H), 7.70 (d, J = 7.6 Hz, 6H), 7.67 (d, J = 8.4 Hz, 4H), 7.62 (m, 6H), 7.57 (m, 6H), 7.38 (d, J = 4.0 Hz, 2H), 7.34 (m, 6H), 7.24 (m, 8H), 4.50 (m, 4H), 3.86−3.81 (m, 11H), 3.75−3.59 (m, 971.1H), 3.55 (m, 8H), 4.46 (t, J = 4.80 Hz, 6H), 3.38 (s, 6H), 2.04 (m, 12H), 1.20−1.09 (m, 60H), 0.80 (t, J = 6.8 Hz, 18H), 0.64 (m, 12H). Elemental analysis (%) calcd for $C_{635.7}H_{1151.4}O_{254.4}S_8$ (13122.2): C 58.19, H 8.84; found: C 58.26, H 9.07.

General Information. Preparative gel-permeation chromatography (PGPC) purification was carried out with a JAI LC-9104 recycling preparative high-performance liquid chromatograph (equipped with JAIGEL 2H/3H column assembly) with toluene as eluent. ^{1}H NMR spectra were recorded on Bruker AV 300 or 400 MHz spectrometers in $CDCl_3$ at 25 °C. Chemical shifts are given in ppm with TMS as reference. Elemental analysis was carried out on a FlashEA1112 elemental analysis system. Gel-permeation chromatography (GPC) measurements were conducted on a Waters 510 system using polystyrene as standard and THF as eluent. Matrix-assisted laser desorption ionization time-of-flight (MALDI-TOF) mass spectra were recorded on a Shimadzu/Kratos AXIMA-CFR MALDI mass spectrometer with anthracene-1,8,9-triol as the matrix. Differential scanning calorimetry (DSC) measurements were performed on TA Q100 thermal analyzer at a scanning rate of 10 °C min^{-1}. UV−vis absorption and photoluminescence (PL) spectra were recorded on a Shimadzu UV3600 spectrometer and a Perkin-Elmer LS 50B luminescence spectrometer, respectively. For PL measurements, the maximum absorption wavelengths were chosen as their corresponding excitation wavelengths. Optical micrographs were taken from an Olympus B51 microscope equipped with an Olympus digital camera. Polarizing optical microscopic observation was conducted on an Olympus BX51 polarizing optical microscope equipped with a LTS 350 hot stage and a TMS 94 temperature programmer (Linkam). Small-angle X-ray scattering (SAXS) was recorded on a Bruker Nanostar instrument operated at 40 kV and 35 mA. Wide-angle X-ray diffraction (WAXD) was performed on Bruker D8 Discover reflector with X-ray generation power of 40 kV tube voltage and 40 mA tube current. Atomic force microscopy (AFM) measurements were performed in tapping mode on a SPA400HV instrument with an SPI 3800 controller (Seiko Instruments).

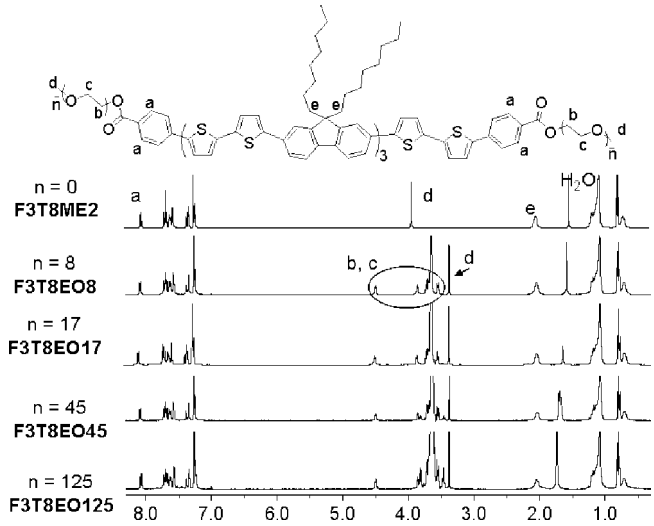

Figure 1. ^{1}H NMR spectra (400 MHz, $CDCl_3$) of PEO-*b*-OFbT-*b*-PEO triblock copolymers **F3T8EO8**, **F3T8EO17**, **F3T8EO45**, and **F3T8EO125** and reference compound **F3T8ME2**. The intensity of PEO proton resonance is cut off for clarity.

Results and Discussion

Synthesis and Structural Characterization. The synthetic route of triblock copolymers **F3T8EO*n*** (n = 8, 17, 45, 125) and reference compound **F3T8ME2** is outlined in Scheme 1. The first, Stille coupling between compound **1** and methyl 4-iodobenzoate (**2**) gave compound **3** in a yield of 70%. Then **3** reacted with **4** to afford the reference compound **F3T8ME2** in a yield of 66%. We found that acidolysis product of **F3T8ME2** (the oligomer carrying two terminal −COOH groups) exhibited very poor solubility for synthesis of PEO-*b*-OFbT-*b*-PEO triblock copolymers via esterification. Therefore,

Table 1. Molecular Structure Characterizations and Phase Behaviors of PEO-*b*-OFbT-*b*-PEO Triblock Copolymers F3T8EO8, F3T8EO17, F3T8EO45, and F3T8EO125 and Reference Compound F3T8ME2

sample	n^a	$M_{cal}{}^a$	$M_w{}^b$	$M_w/M_n{}^b$	phase behaviors[c,d] heating	cooling
F3T8ME2	0	2093	3000	1.03	G 77.1 N 284.8 (3.5) I	I 282.8 (3.8) N 71.8 G
F3T8EO8	8	2823	5300	1.03	G 52.6 S_A 178.8 (3.2) I	I 174.3 (3.2) S_A 48.1 G
F3T8EO17	17	3605	7000	1.04	K 9.2 (32.4) G 49.1 S_A 175.5 (3.3) I	I 171.9 (3.6) S_A 41.8 G −29.2 (20.0) K
F3T8EO45	45	6068	12500	1.04	H_C 51.5 (79.1) R_M 96.0 (<0.1) S_B 114.3 (0.1) S_A 125.4 (0.1) I	I 125.3 S_A 113 S_B 90 R_M 10.7 (68.5) H_C[e]
F3T8EO125	125	13122	17800	1.22	K 56.4 (157.1) I	I 31.6 (157.8) K

[a] Average number of ethylene oxide units (n) and molecular weight (M_{cal}) calculated based on ^{1}H NMR spectra. [b] Weight-average molecular weight (M_w) and polydispersity index (PDI = M_w/M_n) measured by GPC with THF as the eluent and polystyrene as standard. [c] Transition temperatures (°C) and enthalpy (in parentheses, J/g) were measured by DSC (heating and cooling rate of 10 °C/min). [d] G = glass; N = nematic; I = isotropic; S_A = smectic A; K = crystalline; H_C = hexagonal columnar crystalline; R_M = rectangular columnar liquid crystalline; S_B = smectic B. [e] The phase transition temperatures of **F3T8EO45** on cooling process are measured under the help of temperature-dependent SAXS and POM measurements, as the enthalpy changes of liquid crystalline transitions on DSC cooling scan are too small to be used for the transition identification.

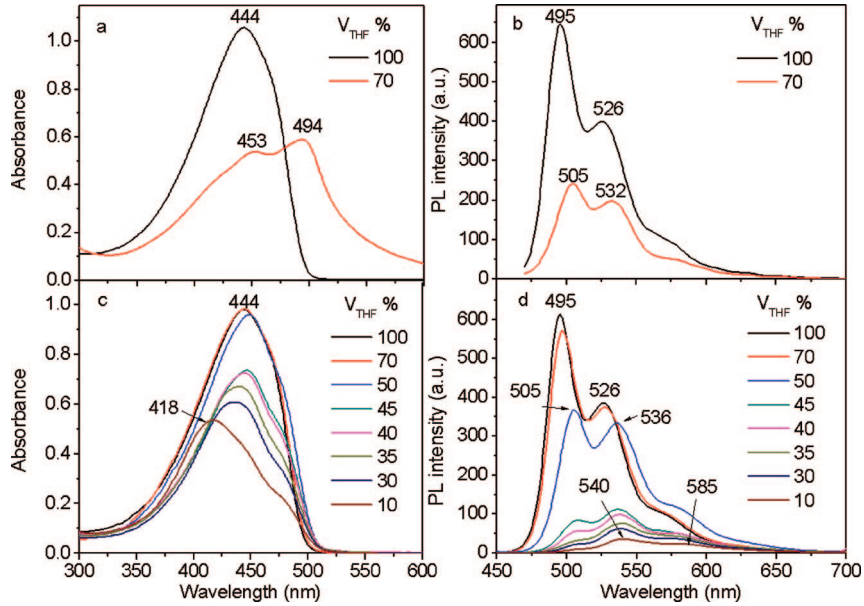

Figure 2. UV−vis absorption and photoluminescence spectra of **F3T8ME2** (a, b) and **F3T8EO17** (c, d) in THF/water mixtures with a concentration of 4×10^{-6} mol/L. The solvent composition is marked by the volume percentage of THF, V_{THF}%.

oligomeric segments **6a**−**d** carrying one PEO coil segment were first synthesized in yields of 75−86%. Finally, triblock copolymers **F3T8EO8**, **F3T8EO17**, **F3T8EO45**, and **F3T8EO125** were prepared via Stille coupling reactions in yields of 30−49%. In order to ensure the purity, these triblock copolymers were further purified by PGPC after common chromatography on silica gel. The chemical structures of the triblock copolymers were confirmed by ^{1}H NMR, GPC, and elemental analysis. Depicted in Figure 1 are ^{1}H NMR spectra of triblock copolymers **F3T8EO*n*** and reference compound **F3T8ME2**. The spectra can be divided into three main regions: aromatic protons at 8.07−7.22 ppm, protons of PEO segement at 4.50−3.38 ppm, and alkyl protons on fluorene units at 2.04−0.64 ppm. Integration ratio of the signals corresponding to H_a, H_e, and $-OCH_3$ protons along with MALDI-TOF mass spectrum or GPC can confirm the structures of **F3T8ME2** and **F3T8EO*n***. On the basis of the integration ratio of $-CH_2CH_2O-$ protons at 4.98−3.38 ppm to $-OCH_3$ protons at 3.37 ppm, the accurate number of the repeating units of PEO block was calculated to be 8, 17, 45, and 125, respectively. As shown in Table 1, all the molecules show a narrow polydispersity as revealed by GPC measurements. Meanwhile, the deviation of GPC measured molecular weight from the calculated ones (M_{cal}) is a general phenomenon for rigid fluorene-based oligomers and polymers, while flexible polystyrene is used as the standard for measurements.[38,39,47,48]

Photophysical Properties. Solution absorption and photoluminescence (PL) spectra were recorded in both THF and THF/water mixture. Since triblock copolymers **F3T8EO*n*** (n = 8, 17, 45, 125) and the reference compound **F3T8ME2** have the same chromophore, comprising three fluorene units, eight thiophene units, and two phenyl units, they exhibited identical absorption (maximum absorption wavelength λ_{max}^{abs} = 444 nm) and PL (maximum emission wavelength λ_{max}^{PL} = 495 nm) spectra in good solvent THF. Meanwhile, both absorption and PL spectra of these compounds in THF are identical to OFbTs with similar length, indicating that ester groups and PEO blocks have a negligible effect on the photophysical properties of the molecules.[39] When water, the good solvent for PEO but bad for conjugated segment, was added, absorption and PL spectra of both **F3T8EO*n*** and **F3T8ME2** were dramatically changed, but in different way. Figure 2 shows the UV−vis absorption and PL spectra of **F3T8ME2** and **F3T8DE17** in THF/water mixtures with different solvent compositions. For easy discussion, the solvent composition of the THF/water mixture is depicted with the THF volume percentage, V_{THF}%. For **F3T8ME2**, before precipitation at V_{THF}% = 70%, both absorption and PL spectra are red-shifted accompanied by an intensity reduction as V_{THF}% decreases, as shown in Figure 2a,b. Meanwhile, the absorption band becomes well resolved instead of a featureless one. This indicates more rigid conformation and the J-type aggregation of the molecules.[49] This phenomenon is

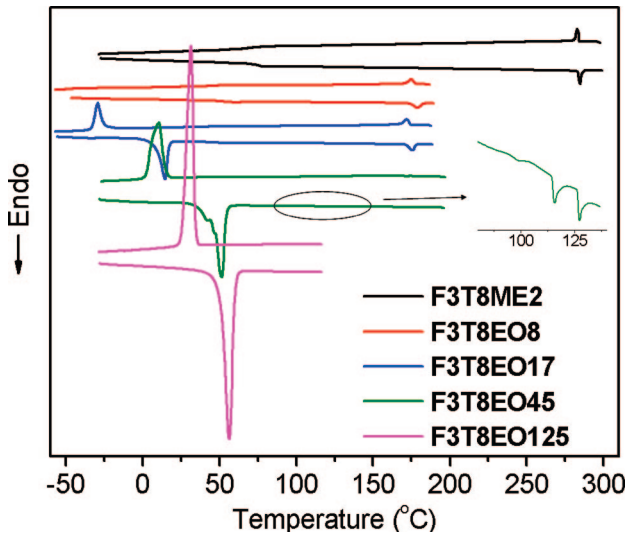

Figure 3. First cooling and the second heating DSC traces of PEO-*b*-OFbT-*b*-PEO triblock copolymers **F3T8EO8**, **F3T8EO17**, **F3T8EO45**, and **F3T8EO125** and reference compound **F3T8ME2** at a heating/cooling rate of ±10 °C min^{-1} in N_2. The inset is the enlarged trace for **F3T8EO45** in the heating scan.

often observed for most conjugated polymers. No obvious precipitation was observed for triblock copolymers **F3T8DE17** even with V_{THF}% as low as 10%, attributed to the presence of PEO blocks. As shown in Figure 2c,d, in addition to the reduced spectra intensity, the UV−vis absorption spectra are first red-shifted and then blue-shifted with a decrease of V_{THF}%, and the critical V_{THF}% is about 45%, while the PL spectra are monotonically red-shifted. At a V_{THF}% of 10%, the blue shift of absorption maximum wavelength is as large as 26 nm, indicative of a strong H-type aggregation of OFbT, as observed in other MCOs-based block copolymers.[9,50] The red shift of the absorption spectrum at initial stage implies that the conjugated segments become more rigid without obvious aggregate formation. As water added, other three triblock copolymers, i.e., **F3T8EO8**, **F3T8EO45**, and **F3T8EO125**, exhibit similar spectroscopic phenomenon. However, it was found that the blue shift of absorption maximum for different triblock copolymers at a similar solvent composition was dependent on f_{PEO} and became smaller with an increase of f_{PEO}, implying a reduced aggregation trend.

Thermotropic Liquid Crystalline Properties. Thermotropic properties of PEO-*b*-OFbT-*b*-PEOs triblock copolymers as characterized by DSC, POM, SAXS, and WAXD are summarized in Table 1. It was found that all compounds except for **F3T8EO125** were mesomorphism. Shown in Figure 3 are the first cooling and the second heating DSC scans of **F3T8EO*n*** and **F3T8ME2** with a heating/cooling rate of ±10 °C min^{-1} in N_2. In the examined temperature ranges, **F3T8ME2** and **F3T8EO8** only exhibit two transitions, corresponding to glass transition and liquid crystalline isotropic transition, respectively. Glass transition temperature (T_g) and liquid crystalline isotropic transition temperature or clearing point (T_c) of **F3T8EO8** are 52.6 and 178.8 °C, respectively, which are lower than 77.1 and 284.8 °C of **F3T8ME2** (Table 1). With an increase of PEO length, T_g and T_c of **F3T8EO17** further decrease to 49.1 and 175.5 °C, respectively. Meanwhile, there is an additional transition at 9.2 °C corresponding to the melting of PEO. **F3T8EO125**, which has the longest PEO coil, is nonmesogenic, and only melting of PEO segment at 56.4 °C was observed. The triblock copolymer **F3T8EO45** exhibits the most complicated thermotropic behavior. Above melting of PEO segment at 51.5 °C, there are three transitions at 96.0, 114.3, and 125.4 °C.

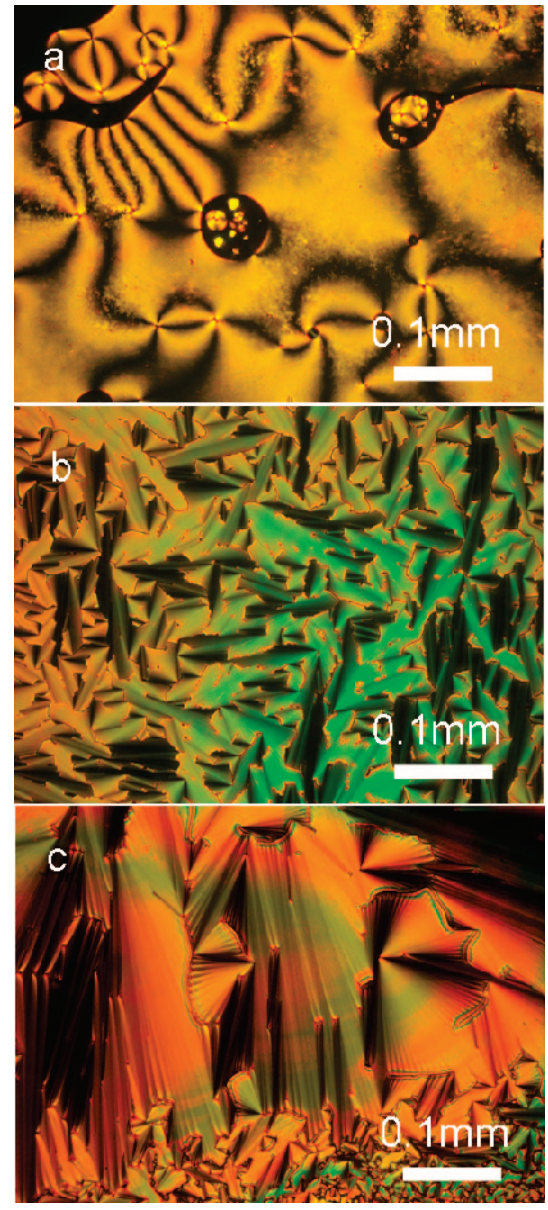

Figure 4. Schlieren textures of **F3T8ME2** at 280 °C (a), the fan textures of **F3T8EO8** at 170 °C (b), and **F3T8EO17** at 144 °C (c) upon cooling from the isotropic state.

To identify the mesophases, **F3T8EO*n*** and **F3T8ME2** were further characterized by POM, SAXS, and WAXD techniques. Like most of the fluorene-based oligomers and polymers,[19,38,39] **F3T8ME2** is nematic mesomorphism, and the nematic Schlieren textures, as shown in Figure 4a, were observed under hot-stage POM of a micrometer-thick film between two glass slides. Meanwhile, there are no peaks in SAXS pattern, and only a diffuse halo in the WAXD pattern is observed, as shown in Figure 5 (SAXS and WAXD patterns of **F3T8ME2** at the temperature between T_g and T_c are identical to the ones at room temperature). This result indicates a glassy−nematic nature of **F3T8ME2**. However, triblock copolymers **F3T8EO*n*** exhibit a distinct behavior. Both **F3T8EO8** and **F3T8EO17**, with f_{PEO} of 0.16 and 0.28, respectively, display smectic A (S_A) mesophase as evidenced by the fan textures typical for S_A mesophase, as shown in Figure 4b,c. SAXS and WAXD measurements also support this assignment. As shown in Figure 5a, the diffraction peaks at $2\theta = 1.07°$ for **F3T8EO8** and 0.87° for **F3T8EO17**, corresponding to the molecular length related *d*-spacings of 8.3 and 10.2 nm, respectively, indicate the layering arrangement

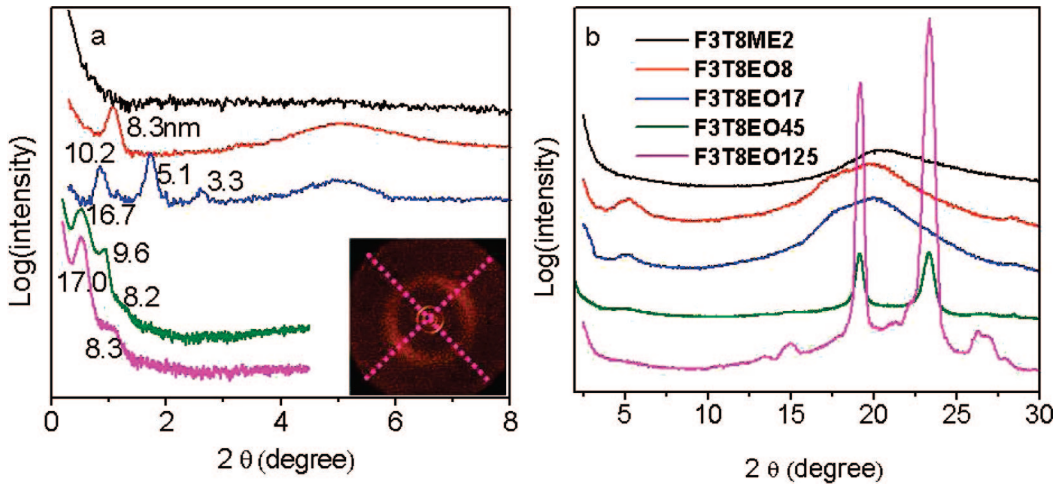

Figure 5. SAXS (a) and WAXD (b) of PEO-*b*-OFT-*b*-PEO triblock copolymers **F3T8EO8**, **F3T8EO17**, **F3T8EO45**, and **F3T8EO125** and reference compound **F3T8ME2** at 25 °C. Inset in (a) is the two-dimensional SAXS of **F3T8EO17** at 25 °C.

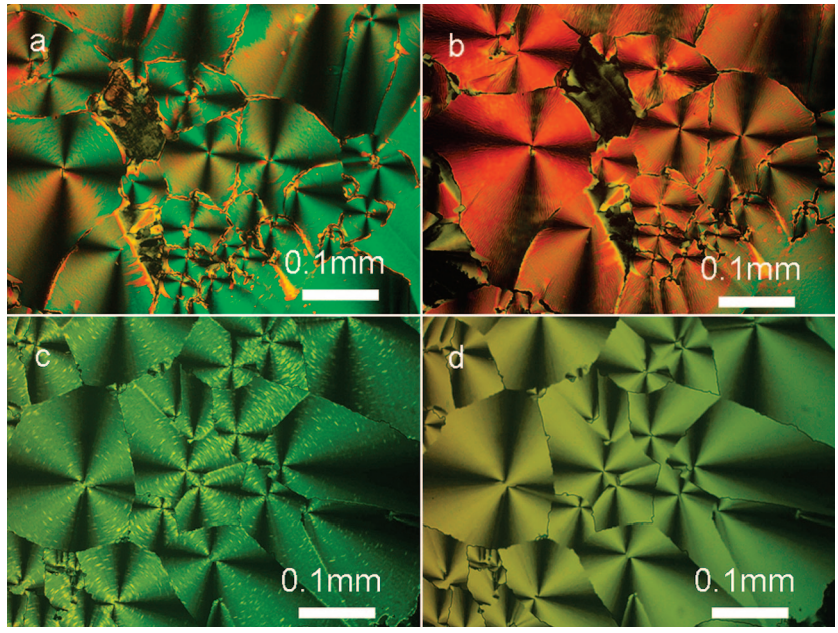

Figure 6. POM images of **F3T8EO45** at 25 (a), 69 (b), 112 (c), and 117 °C (d) on the second heating from 0 °C.

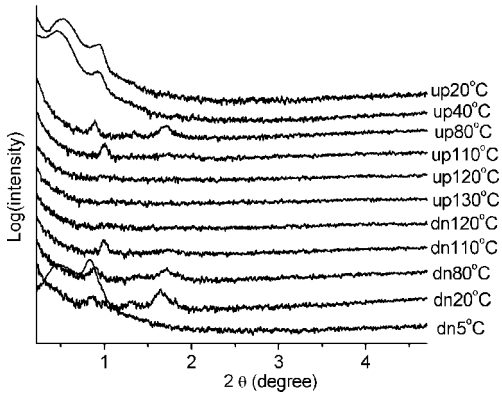

Figure 7. Temperature-dependent SAXS of **F3T8EO45** in the second heating and cooling processes with temperatures labeled on the right-hand side. Up and dn represent heating and cooling, respectively.

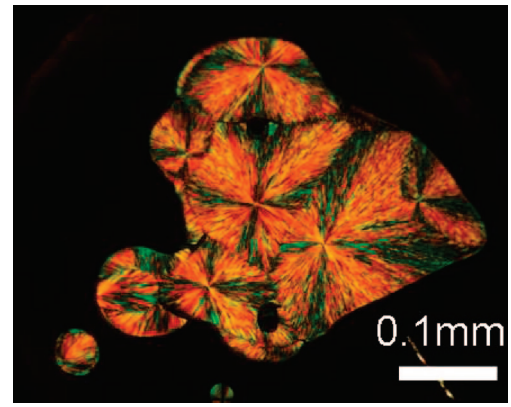

Figure 8. Spherulite texture of **F3T8EO125** at 25 °C upon cooling from the isotropic state.

of the molecules. Although only one peak ($2\theta = 1.07°$) can be observed for **F3T8EO8**, two other diffraction peaks for **F3T8EO17** observed at 1.73° and 2.65° arising from the layering period are due to the second- and third-order diffractions, respectively, indicating an increase of the liquid crystal order along the layering direction as the length of PEO or f_{PEO} increases. The broad peak at $2\theta \sim 5°$, which is in good

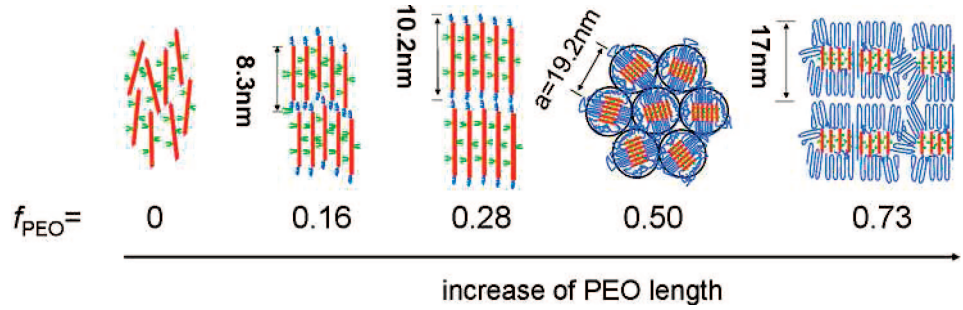

Figure 9. Schematic representation of the molecular arrangement of PEO-*b*-OFbT-*b*-PEO triblock copolymers **F3T8EO8**, **F3T8EO17**, **F3T8EO45**, and **F3T8EO125** and reference compound **F3T8ME2** at room temperature. For calculation of the volume fraction of PEO (f_{PEO}), the densities of OFbT and PEO segments were assumed as 1.14 and 1.13 g/cm^3, respectively.[43,44]

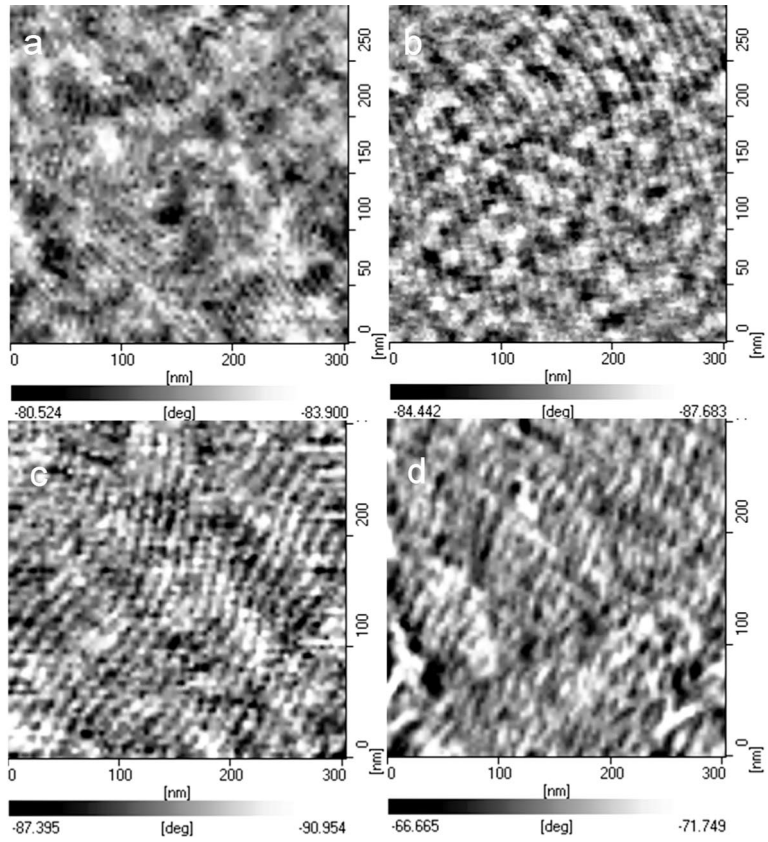

Figure 10. Tapping mode AFM phase images of **F3T8EO8** (a), **F3T8EO17** (b), **F3T8EO45** (c), and **F3T8EO125** (d) films spin-cast from 3 mg/mL $CHCl_3$ solution at 1000 rpm on quartz. Films were first annealed at isotropic state for 10 min, then at liquid crystalline state for 20 min, and finally cooled to room temperature for measurements, except that **F3T8EO45** film was further cooled to 0 °C and kept for 60 min for crystallization of PEO block and then warmed to room temperature for measurements.

agreement with lateral packing of OFbT blocks,[51,52] implies the presence of the weak inner-layer order. The S_A mesophase is further solidified by the two-dimensional SAXS patterns recorded with a slightly sheared sample. The inset of Figure 5a is a typical two-dimensional SAXS pattern of **F3T8EO17** as an example. Two sets of diffractions at 0.87° and ~5° are almost along two perpendicular directions. This is typical for S_A mesophase. A diffuse halo at 15°−25° is observed, which is consistent with the liquid crystalline state of the triblock copolymers **F3T8EO8** and **F3T8EO17**, as shown in Figure 5b.

Further increasing PEO length to f_{PEO} of 0.50 for **F3T8EO45** induces more complex phase transitions and the formation of higher order mesophases. Figure 6 and Figure 7 show POM images and SAXS patterns of **F3T8EO45**, respectively, at different temperatures. For POM observations and SAXS measurements, the sample was first heated to isotropic state and then slowly cooled to 0 °C for crystallization. At 25 °C, the pseudo-focal-conic textures with broken borderlines are observed as shown in Figure 6a. Meanwhile, diffractions with *d*-spacing values of $1:{}^1/_{\sqrt{3}}:{}^1/_2$ in SAXS and the sharp diffraction peaks at 19.2° and 23.4° as shown in WAXD (Figure 5b), characteristic for crystalline PEO, are observed at 20 °C upon heating. These results indicate a columnar hexagonal crystalline phase with lattice parameter $a = 19.2$ nm. The presence of diffraction peak at $2\theta \sim 5°$ suggests that the conjugated rods are laterally packed in columns. When temperature exceeds 51.5 °C, PEO blocks melt and three liquid crystalline phases appear in succession. The first mesophase between 51.5 and 96.0 °C is identified as a columnar rectangular liquid crystalline phase for the presence of the fan texture with radiating straight lines across the fan length (Figure 6b) and diffraction peaks with *d*-spacing values of $1:{}^1/_{1.5}:{}^1/_2$ in SAXS (Figure 7). At temperature between 96.0 and 114.3 °C, a fan texture with transitional concentric arcs indicates a smectic B (S_B) mesophase,[53,54] although only one

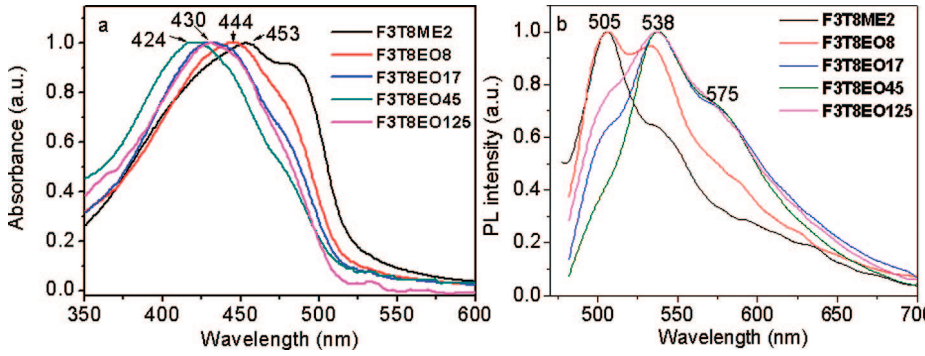

Figure 11. Film UV−vis absorption and PL spectra of PEO-*b*-OFbT-*b*-PEO triblock copolymers **F3T8EO8**, **F3T8EO17**, **F3T8EO45**, and **F3T8EO125** and reference compound **F3T8ME2** on quartz. For PL measurements, the samples were excited at absorption maximum. Film preparation is identical to that for AFM measurements.

diffraction peak appears in SAXS. The last liquid crystal phase is defined as S_A for the typical fan texture, although no obvious diffraction peak has been observed due to the low order of the structure which can also be presumed from the small enthalpy change in DSC measurement (Table 1). In DSC cooling curve, the liquid crystalline transition peaks cannot be distinguished from the noise for the too small enthalpy changes. Fortunately, these transitions can be observed by temperature-dependent SAXS and POM.

When f_{PEO} rises to 0.73, spherulite texture (Figure 8) and lamellar diffraction pattern in SAXS (Figure 5a) of **F3T8EO125** similar to PEO homopolymer indicate that crystallization of PEO blocks dominates the phase structure for this triblock copolymer. The interaction between conjugated blocks along the alkyl direction almost disappears as no diffraction observed around 5° in WAXD (Figure 5b). The relative intensity of this diffraction decreases as f_{PEO} increases from **F3T8EO8** to **F3T8EO125** which can be attributed to the steric hindrance of bulk PEO blocks.[11]

According to the above discussion, the arrangement of the molecules with different f_{PEO} at room temperature is summarized in Figure 9. With f_{PEO} increases from 0 to 0.73, phase structures change from nematic to smectic, hexagonal columnar, and then lamellar nanostructures. From the scheme, it is obvious that the introduction of the PEO block can lead to highly ordered mesophases, from nematic to smectic liquid crystals. Larger f_{PEO} (from 0.16 to 0.28) enhances the correlation between layers in smectic liquid crystals. When f_{PEO} increases to 0.50, unconventional nanostructures such as columnar phases have been observed. From lamellar to columnar phase by simply change the coil volume fraction has also been achieved in phenylene/fluorene/thiophene hybride oligomer based triblock copolymers.[13] However, when f_{PEO} increases to 0.73, the lateral interaction between the conjugated rods along the alkyl direction is disrupted for the bulk steric hindrance of long PEO blocks.

Thin Film Morphology. Based on the above discussion, these triblock copolymers should be capable of forming nanostructured films. Therefore, the film morphology was studied by AFM. In order to eliminate the effect of process condition, the spin-cast films with the thickness of about 25 nm were annealed first at the isotropic state for 10 min and then liquid crystalline state for 20 min, except that **F3T8EO45** film was further cooled to 0 °C and kept for 60 min for crystallization of PEO block and then warmed to room temperature for measurements. Figure 10 shows the tapping mode AFM phase images of the annealed thin films. For all triblock copolymers, alternative bright-dark stripes are observed, except for **F3T8EO8** which only exhibits locally lamellar ordering with a short persistence length of about 60 nm probably due to the weakest phase separation originated from the lowest f_{PEO}. The lengths of the stripes in **F3T8EO125** film are relatively shorter due to the disruption of the long-range interaction between the conjugated rod segments by the bulk PEO.[26] The measured periods of these stripes, 9 ± 1, 11 ± 1, and 17 ± 3 nm for **F3T8EO8**, **F3T8EO17**, and **F3T8EO125**, respectively, are all comparable to the corresponding layer distances observed in SAXS at room temperature (Figure 5a), considering the fat tip effect in AFM measurements. While the spacing for **F3T8EO45** thin film is 16 ± 3 nm, which is related to the repeated period of $(\sqrt{3}/2)a$ observed as the first diffraction peak in SAXS. Only $(\sqrt{3}/2)a$ repeated period is visualized, which may be ascribed to the planar alignment of columns on the substrate. Clearly, the above nanostructures are correlated with molecular length and coil/rod ratio, demonstrating the advantages of MCOs for triblock copolymers forming well-defined nanostructures.

Film spectroscopic properties of the triblock copolymers are consistent with the formation of the above nanostructures, as shown in Figure 11. Compared to those in dilute THF solution, the maximum absorption and emission wavelengths of **F3T8ME2** film are both red-shifted, from 444 to 453 nm and 495 to 505 nm, respectively. In contrast, film absorption spectra of **F3T8EO17**, **F3T8EO45**, and **F3T8EO125** exhibit blue shifts of 14, 20, and 14 nm, respectively. The maximum absorption wavelength of **F3T8EO8** film is identical to that in THF solution, which may be due to a compromise between planarization and H-aggregation of the conjugated segments, and is consistent with its shortest PEO length. A smaller blue shift of **F3T8EO125** than **F3T8EO45** is ascribed to the bulky steric hindrance of PEO, which can reduce the interaction between conjugated segments. The emission spectra of PEO-*b*-OFbT-*b*-PEO triblock copolymers are also red-shifted compared to those in dilute THF solution, but different from that of **F3T8ME2**, the intensities at long wavelengths, 538 and 575 nm, are relatively increased as PEO length increases. Larger f_{PEO} display stronger relative intensities at these two long wavelengths. A similar film spectroscopic phenomenon has been also observed in phenylenevinylene-based rod−coil block copolymers, but no film morphology has been reported.[11]

Conclusion

A series of PEO-*b*-OFbT-*b*-PEO triblock copolymers **F3T8EO8**, **F3T8EO17**, **F3T8EO45**, and **F3T8EO125** with f_{PEO} of 0.16, 0.28, 0.50, and 0.73, respectively, were synthesized, and their f_{PEO}-dependent photophysical properties, thermotropic liquid crystalline properties, and film morphology were studied. A reference compound with the identical rod but without PEO, **F3T8ME2**, was also prepared for comparison. The introduction of PEO into the triblock block copolymers encourages the formation of H-type aggregation and highly ordered mesophases while $f_{PEO} < 0.73$. **F3T8ME2**, which does not carry PEO block,

is nematic mesomorphism. In contrast, **F3T8EO8** and **F3T8EO17** are S_A mesomorphism. With further increase of f_{PEO} to 0.50 for **F3T8EO45**, several highly ordered phases including hexagonal columnar crystalline phase, and rectangular columnar, S_B and S_A mesophases appear in succession upon heating. However, large volume fraction of coil segments suppresses the formation of mesophase. For **F3T8EO125** with $f_{PEO} = 0.73$, only a crystalline phase was observed. Meanwhile, thin films of above triblock copolymers exhibit lamellar or cylindrical nanostructures correlated with phase structures at room temperature, which renders the block copolymers different spectroscopic properties.

Acknowledgment. This work is supported by NSFC (Nos. 20621401 and 20521415) and MOST of China (2009CB930603).

References and Notes

(1) Hoeben, F. J. M.; Jonkheijm, P.; Meijer, E. W.; Schenning, A. P. H. J. *Chem. Rev.* **2005**, *105*, 1491–1546.
(2) Klok, H.-A.; Lecommandoux, S. *Adv. Mater.* **2001**, *13*, 1217–1229.
(3) Lee, M.; Cho, B.-K.; Zin, W.-C. *Chem. Rev.* **2001**, *101*, 3869–3892.
(4) Liang, Y. Y.; Wang, H. B.; Yuan, S. W.; Lee, Y. G.; Gan, L.; Yu, L. P. *J. Mater. Chem.* **2007**, *17*, 2183–2194.
(5) Olsen, B. D.; Segalman, R. A. *Mater. Sci. Eng., R* **2008**, *62*, 37–66.
(6) Ryu, J.-H.; Lee, M. *Struct. Bond. (Berlin)* **2008**, *128*, 63–98.
(7) Lee, M.; Yoo, Y.-S. *J. Mater. Chem.* **2002**, *12*, 2161–2168.
(8) (a) Tenneti, K. K.; Chen, X. F.; Li, C. Y.; Wan, X. H.; Fan, X. H.; Zhou, Q. F.; Rong, L. X.; Hsiao, B. S. *Soft Matter* **2008**, *4*, 458–461. (b) Tenneti, K. K.; Chen, X. F.; Li, C. Y.; Tu, Y. F.; Wan, X. H.; Zhou, Q. F.; Sics, I.; Hsiao, B. S. *J. Am. Chem. Soc.* **2005**, *127*, 15481–15490. (c) Liu, X. B.; Zhao, Y. F.; Chen, E. Q.; Ye, C.; Shen, Z. H.; Fan, X. H.; Cheng, S. Z. D.; Zhou, Q. F. *Macromolecules* **2008**, *41*, 5223–5229.
(9) Wang, H. B.; Wang, H. H.; Urban, V. S.; Littrell, K. C.; Thiyagarajan, P.; Yu, L. P. *J. Am. Chem. Soc.* **2000**, *122*, 6855–6861.
(10) Wang, H. B.; You, W.; Jiang, P.; Yu, L. P.; Wang, H. H. *Chem.—Eur. J.* **2004**, *10*, 986–993.
(11) Hulvat, J. F.; Sofos, M.; Tajima, K.; Stupp, S. I. *J. Am. Chem. Soc.* **2005**, *127*, 366–372.
(12) Lee, E.; Ryu, J.-H.; Park, M.-H.; Lee, M.; Han, K.-H.; Chung, Y.-W.; Cho, B.-K. *Chem. Commun.* **2007**, 2920–2922.
(13) Lin, H.-C.; Lee, K.-W.; Tsai, C.-M.; Wei, K.-H. *Macromolecules* **2006**, *39*, 3808–3816.
(14) Chen, S. A.; Lu, H. H.; Huang, C. W. *Adv. Polym. Sci. (Berlin)* **2008**, *212*, 49–84.
(15) Wallace, J. U.; Chen, S. H. *Adv. Polym. Sci. (Berlin)* **2008**, *212*, 145–186.
(16) Monkman, A.; Rothe, C.; King, S.; Dias, F. *Adv. Polym. Sci. (Berlin)* **2008**, *212*, 187–225.
(17) Leclerc, M. *J. Polym. Sci., Polym. Chem.* **2001**, *39*, 2867–2873.
(18) Scherf, U.; List, E. J. W. *Adv. Mater.* **2002**, *14*, 477–487.
(19) Neher, D. *Macromol. Rapid Commun.* **2001**, *22*, 1365–1385.
(20) Allard, S.; Forster, M.; Souharce, B.; Thiem, H.; Scherf, U. *Angew. Chem., Int. Ed.* **2008**, *47*, 4070–4098.
(21) Thompson, B. C.; Fréchet, J. M. J. *Angew. Chem., Int. Ed.* **2008**, *47*, 58–77.
(22) Marsitzky, D.; Klapper, M.; Müllen, K. *Macromolecules* **1999**, *32*, 8685–8688.
(23) Lu, S.; Fan, Q.-L.; Liu, S.-Y.; Chua, S.-J.; Huang, W. *Macromolecules* **2002**, *35*, 9875–9881.
(24) Lu, S.; Fan, Q.-L.; Chua, S.-J.; Huang, W. *Macromolecules* **2003**, *36*, 304–310.
(25) Kong, X. X.; Jenekhe, S. A. *Macromolecules* **2004**, *37*, 8180–8183.
(26) Surin, M.; Marsitzky, D.; Grimsdale, A. C.; Müllen, K.; Lazzaroni, R.; Leclère, P. *Adv. Funct. Mater.* **2004**, *14*, 708–715.
(27) Wang, F. *Mater. Lett.* **2006**, *60*, 2933–2936.
(28) Nomura, K.; Yamamoto, N.; Ito, R.; Fujiki, M.; Geerts, Y. *Macromolecules* **2008**, *41*, 4245–4249.
(29) Rubatat, L.; Kong, X. X.; Jenekhe, S. A.; Ruokolainen, J.; Hojeij, M.; Mezzenga, R. *Macromolecules* **2008**, *41*, 1846–1852.
(30) Tsolakis, P. K.; Kallitsis, J. K. *Chem.—Eur. J.* **2003**, *9*, 936–943.
(31) Chochos, C. L.; Tsolakis, P. K.; Gregoriou, V. G.; Kallitsis, J. K. *Macromolecules* **2004**, *37*, 2502–2510.
(32) Chochos, C. L.; Kallitsis, J. K.; Gregoriou, V. G. *J. Phys. Chem. B* **2005**, *109*, 8755–8760.
(33) Zhang, Z.-J.; Qiang, L.-L.; Liu, B.; Xiao, X.-Q.; Wei, W.; Peng, B.; Huang, W. *Mater. Lett.* **2006**, *60*, 679–684.
(34) Xiao, X.; Fu, Y.-Q.; Zhou, J.-J.; Bo, Z.-S.; Li, L.; Chan, C.-M. *Macromol. Rapid Commun.* **2007**, *28*, 1003–1009.
(35) (a) Martin, R. E.; Diederich, F. *Angew. Chem., Int. Ed.* **1999**, *38*, 1350–1377. (b) Müllen, K.; Wegner, G. *Electronic Materials: The Oligomer Approach*; Wiley-VCH: Weinheim, NY, 1998. (c) Gierschner, J.; Cornil, J.; Egelhaaf, H.-J. *Adv. Mater.* **2007**, *19*, 173–191.
(36) Geng, Y. H.; Trajkovska, A.; Katsis, D.; Ou, J. J.; Culligan, S. W.; Chen, S. H. *J. Am. Chem. Soc.* **2002**, *124*, 8337–8347.
(37) Geng, Y. H.; Culligan, S. W.; Trajkovska, A.; Wallace, J. U.; Chen, S. H. *Chem. Mater.* **2003**, *15*, 542–549.
(38) Liu, Q.; Liu, W. M.; Yao, B.; Tian, H. K.; Xie, Z. Y.; Geng, Y. H.; Wang, F. S. *Macromolecules* **2007**, *40*, 1851–1857.
(39) Zhang, X. J.; Qu, Y.; Bu, L. J.; Tian, H. K.; Zhang, J. P.; Wang, L. X.; Geng, Y. H.; Wang, F. S. *Chem.—Eur. J.* **2007**, *13*, 6238–6248.
(40) Güntner, R.; Farrell, T.; Scherf, U.; Miteva, T.; Yasuda, A.; Nelles, G. *J. Mater. Chem.* **2004**, *14*, 2622–2626.
(41) Sirringhaus, H.; Wilson, R. J.; Friend, R. H.; Inbasekaran, M.; Wu, W.; Woo, E. P.; Grell, M.; Bradley, D. D. C. *Appl. Phys. Lett.* **2000**, *77*, 406–408.
(42) Sirringhaus, H.; Kawase, T.; Friend, R. H.; Shimoda, T.; Inbasekaran, M.; Wu, W.; Woo, E. P. *Science* **2000**, *290*, 2123–2126.
(43) Destri, S.; Pasini, M.; Botta, C.; Porzio, W.; Bertini, F.; Marchiò, L. *J. Mater. Chem.* **2002**, *12*, 924–933.
(44) Takahashi, Y.; Tadokoro, H. *Macromolecules* **1973**, *6*, 672–675.
(45) Moore, J. S.; Stupp, S. I. *Macromolecules* **1990**, *23*, 65–70.
(46) Messmore, B. W.; Hulvat, J. F.; Sone, E. D.; Stupp, S. I. *J. Am. Chem. Soc.* **2004**, *126*, 14452–14458.
(47) Grell, M.; Bradley, D. D. C.; Long, X.; Chamberlain, T.; Inbasekaran, M.; Woo, E. P.; Soliman, M. *Acta Polym.* **1998**, *49*, 439–444.
(48) Liu, Q.; Qu, Y.; Geng, Y. H.; Wang, F. S. *Macromolecules* **2008**, *41*, 5964–5966.
(49) Siddiqui, S.; Spano, F. C. *Chem. Phys. Lett.* **1999**, *308*, 99–105.
(50) Li, K.; Guo, L.; Liang, Z.; Thiyagarajan, P.; Wang, Q. *J. Polym. Sci., Polym. Chem.* **2005**, *43*, 6007–6019.
(51) Li, N.; Zhang, X. J.; Geng, Y. H.; Su, Z. H. *Macromol. Chem. Phys.* **2008**, *209*, 1806–1813.
(52) Li, N.; Zhang, X. J.; Geng, Y. H.; Su, Z. H. *Polymer* **2008**, *49*, 4279–4284.
(53) Gray, G. W.; Goodby, J. W. G. *Smectic Liquid Crystals;Textures and Structures*; Leonard Hill: Glasgow, 1984.
(54) Dierking, I. *Textures of Liquid Crystals*; Wiley-VCH: Weinheim, 2003.

MA802601C